

Reconfinement shocks in relativistic AGN jets

Krzysztof Nalewajko and Marek Sikora

Nicolaus Copernicus Astronomical Center, ul. Bartycka 18, 00-716 Warsaw, Poland

Abstract. Stationary knots observed in many AGN jets can be explained in terms of a reconfinement shock that forms when relativistic flow of the jet matter collides with the external medium. The position of these knots can be used, together with information on external pressure profile, to constrain dynamical parameters of the jet. We present a semi-analytical model for the dynamical structure of reconfinement shocks, taking into account exact conservation laws both across the shock surface and in the zone of the shocked jet matter. We show that, due to the transverse pressure gradient in the shock zone, the position of the reconfinement is larger than predicted by simple models. A portion of kinetic energy is converted at the shock surface to internal energy, with efficiency increasing strongly with both bulk Lorentz factor of the jet matter and the jet half-opening angle. Our model may be useful as a framework for modeling non-thermal radiation produced within the stationary features.

Keywords: galaxies: jets – shock waves

PACS: 98.62.Nx, 52.35.Tc

INTRODUCTION

Interaction between AGN jet and its environment leads to formation of a reconfinement shock [1]. Such shocks have been considered to be responsible for non-thermal activity in AGN radio cores [2] and, on much larger distances, in kiloparsec-scale radio knots [3].

The connection between geometrical properties of the shock surface and physical matter parameters has been studied in [4]. Under many simplifying assumptions they provided simple analytical formulae. In order to test their predictions, we have developed two models based on exact conservation laws for ideal relativistic gas. Assuming static external medium, we only have one shocked zone bounded with the shock surface $r_s(z)$ and contact discontinuity $r_c(z)$. This basic structure is shown in Fig. 1. The jet is launched from the vicinity of the central source with a half-opening angle Θ_j , it achieves its maximum width r_m at $z = z_m$, then it reconfines at $z = z_r$ with a half-closing angle Θ_r .

The parameters needed to describe a model are: jet bulk Lorentz factor Γ_j , initial half-opening angle Θ_j , kinetic power L_j , external pressure $p_e(z)$, specific heats ratio of the shocked matter γ_s . Given the flow parameters of the jet and the external medium, we calculate the flow parameters of the shocked zone and the inclination angles of the boundary surfaces.

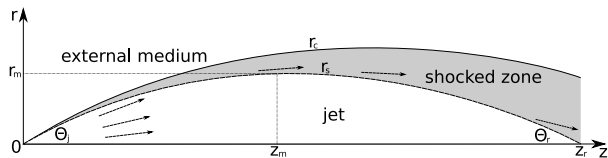


FIGURE 1. Structure of the reconfinement shock for static external medium.

Model 1. is based on assumption that the shocked zone has no transverse structure, therefore the pressure behind the shock is equal to the external pressure ($p_s = p_e$). The flow parameters behind the shock are found by solving the exact relativistic shock-jump equations. The velocity field across the shocked zone is assumed to be parallel to the solution obtained just behind the shock surface for a given z . The contact discontinuity surface is obtained as the outline of the velocity field. In result, we have found that under such approximations the mass flux conservation across the shocked zone is violated.

Model 2. includes transverse structure of the shocked zone. Parameters just behind the shock are treated as independent of the parameters at the contact discontinuity. To compensate for 4 additional degrees of freedom, the full set of conservation laws across the shocked zone, based on [5], are introduced into the scheme. The profiles of pressure and density across the zone are approximated with linear functions of r .

SHOCK GEOMETRY

We present here the results obtained assuming cold jet (of negligible pressure) and uniform external pressure. In the model of [4], under such conditions the jet boundary is expected to be parabolic. Position of the reconfinement can be estimated as:

$$z_r \simeq \Lambda \equiv \sqrt{\frac{\mu \beta_j L_j}{\pi p_e c}}, \quad (1)$$

where $\mu = 17/24$. Consequently, we expect $r_m/z_r \simeq \Theta_j/4$, $z_m \simeq z_r/2$ and $\Theta_r \simeq \Theta_j$.

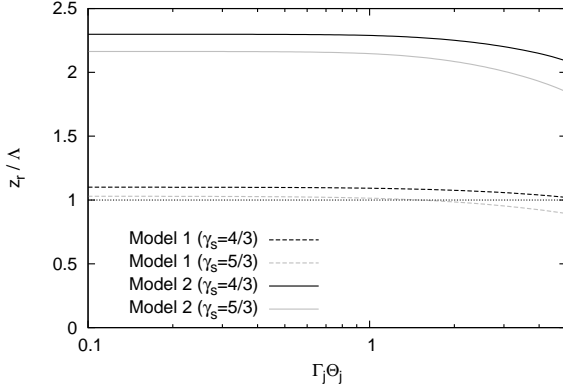


FIGURE 2. The ratio of reconfinement position z_r to the characteristic length Λ as a function of $\Gamma_j \Theta_j$. Results for Model 1 (*dashed lines*) and Model 2 (*solid lines*) are shown for different equations of state of the shocked matter: $\gamma_s = 4/3$ (*black lines*) and $\gamma_s = 5/3$ (*grey lines*).

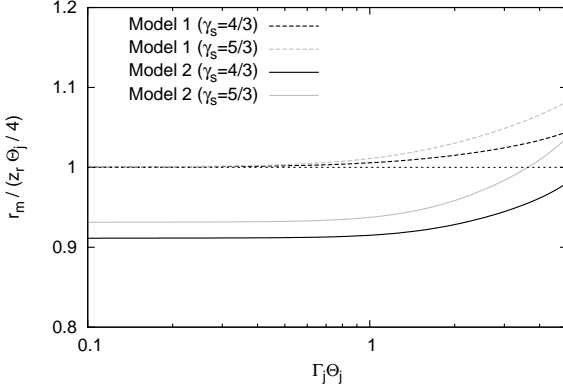


FIGURE 3. The aspect ratio of unshocked jet r_m/z_r , divided by the value $\Theta_j/4$ predicted by [4], as a function of $\Gamma_j \Theta_j$. The linestyles are the same as in Fig. 2.

We have tested these predictions in both our models with the same parameters. We have generally found that the parameters that we tested, are functions of the product of Γ_j and Θ_j . As the two extreme states of shocked matter, we consider the relativistic limit $\gamma_s = 4/3$ and the non-relativistic limit $\gamma_s = 5/3$.

The z_r/Λ , r_m/z_r , z_r/z_m and Θ_r/Θ_j ratios, calculated for $\Gamma_j = 10$ and varying Θ_j , are shown in Figs. 2 – 5, respectively. We find, that Model 1 agrees very well with the results of [4] for $\Gamma_j \Theta_j < 1$ and is still in reasonable agreement otherwise. Model 2 produces a jet more than twice longer, with the aspect ratio r_m/z_r smaller than $\Theta_j/4$, the maximum width position z_m closer than $z_r/2$ and the half-closing angle Θ_r smaller than Θ_j .

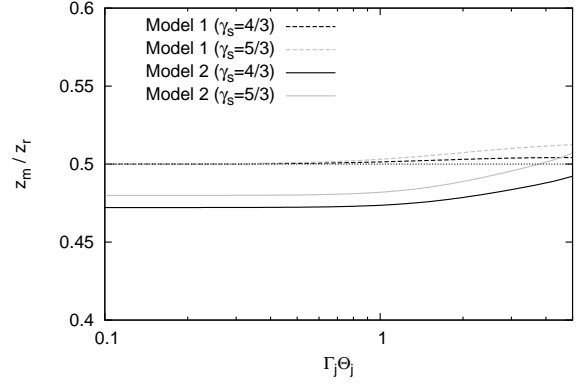


FIGURE 4. The ratio of the maximum jet width position z_m to the reconfinement position z_r as a function of $\Gamma_j \Theta_j$. The linestyles are the same as in Fig. 2.

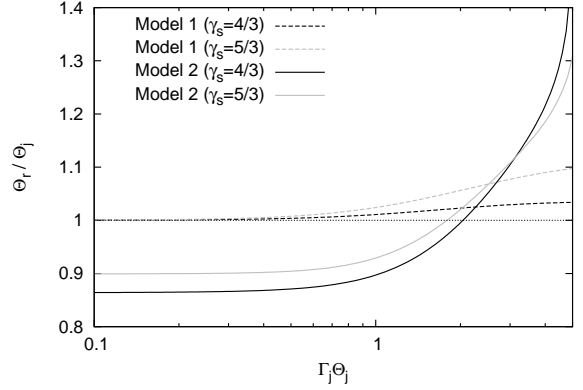


FIGURE 5. The ratio of the half-closing angle Θ_r to the half-opening angle Θ_j as a function of $\Gamma_j \Theta_j$. The linestyles are the same as in Fig. 2.

ENERGY DISSIPATION

Kinetic energy of the cold jet matter crossing the shock surface is dissipated with efficiency

$$\epsilon_{diss} = \frac{\Gamma_j - \Gamma_s}{\Gamma_j - 1}. \quad (2)$$

Fig. 6 shows this efficiency calculated in our models with the same parameters as before. The results from the two models are very similar, we find that ϵ_{diss} depends strongly on $\Gamma_j \Theta_j$, achieving values higher than 6% for $\Gamma_j \Theta_j > 1$.

Although the total flux of dissipated energy produced in the two models is similar, its geometrical distribution is different. Fig. 7 shows the flux of dissipated energy per unit jet length dL_{diss}/dz for the two models for $\Gamma_j = 10$ and $\Theta_j = 5^\circ$. The dependence of the location of the

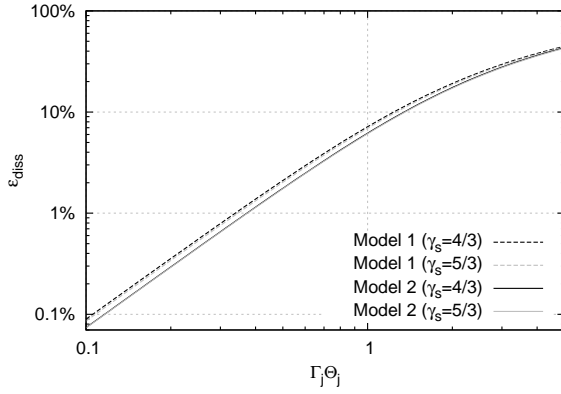


FIGURE 6. Dissipation efficiency ϵ_{diss} as a function of $\Gamma_j \Theta_j$, calculated for $\Gamma_j = 10$. The linestyles are the same as in Fig. 2.

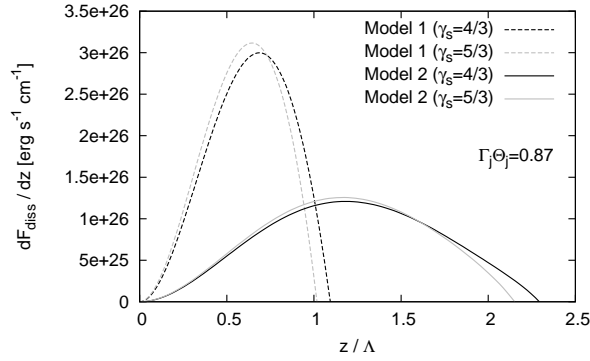


FIGURE 7. Profiles of dissipated energy flux produced at the shock surface, calculated for $\Gamma_j = 10$ and $\Theta_j = 5^\circ$. The linestyles are the same as in Fig. 2.

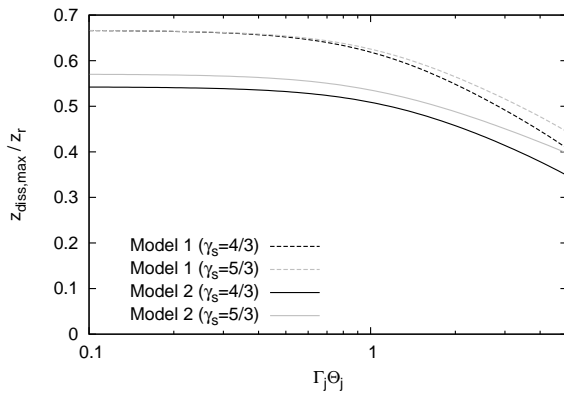


FIGURE 8. Ratio of the location of maximum of dissipated energy $z_{diss,max}$ to the reconfinement position z_r as a function of $\Gamma_j \Theta_j$. The linestyles are the same as in Fig. 2.

dissipated energy flux maximum on $\Gamma_j \Theta_j$ is shown in Fig. 8. The $z_{diss,max}/z_r$ ratio is smaller in Model 2 and it strongly decreases in both models for $\Gamma_j \Theta_j > 1$.

ACKNOWLEDGMENTS

The present work was partially supported by the Polish Astroparticle Network 621/E-78/SN-0068/2007.

REFERENCES

1. Sanders, R. H., 1983, ApJ, 266, 73
2. Daly, R. A., & Marscher, A. P., 1988, ApJ, 334, 539
3. Komissarov, S. S., & Falle, S. A. E. G., 1998, MNRAS, 297, 1087
4. Komissarov, S. S., & Falle, S. A. E. G., 1997, MNRAS, 288, 833 (KF97)
5. Bromberg, O., & Levinson, A., 2007, ApJ, 671, 678, arXiv:0705.2040